remote sensing

MDPI

Article

Integrating Commercial and Public Imagery to Accelerate Deforestation Alerts

Zhiqiang Yang [1], Eric L. Bullock [2], Erik J. Lindquist [3], Carole Andrianirina [4] and Sean P. Healey [1,*]

1 USDA Rocky Mountain Research Station, 4919 S 1500 W, Ste. 200, Riverdale, UT 84405, USA; zhiqiang.yang@usda.gov
2 School of Biological Sciences, University of Utah, 257 S 1400 E Rm 201, Salt Lake City, UT 84112, USA; e.bullock@utah.edu
3 UN Food and Agriculture Organization, Viale delle Terme di Caracalla, 00153 Rome, Italy; erik.lindquist@fao.org
4 Laboratoire d'Observation des Forets de Madagascar (LOFM), Bureau National de Coordination des Changements Climatiques et de la REDD+ (BNCCREDD+), Ministere de l'Environnement et du Developpement Durable, Rue Toto Radola Antsahavola, Antananarivo 101, Madagascar; andrianirinacarole59bis@gmail.com
* Correspondence: sean.healey@usda.gov

Highlights

What are the main findings?

- Tests in Madagascar's frequently cloudy primary forests showed that using PlanetScope imagery alone with DIAS allowed detection of 52% of deforestation at the 10 m scale within a month, and that use of PlanetScope plus public sensors boosted detection to 68% with a false-alarm rate of approximately 20%.
- A controlled experiment with Landsat and Sentinel-2 data over the test sites demonstrated that allowing imagery from different sensors to corroborate each other in building alert confidence produces a significant alert latency advantage in the first five weeks after deforestation over current methods that require corroboration of change detected in one image to come from subsequent imagery from the same source.

What are the implications of the main findings?

- The apparent coherence of DI values from diverse sources in the context of DIAS' multi-sensor change detection algorithm, as well as effective use of 2022 Landsat-7 data acquired at varying altitudes and overpass times, suggest robustness to sensor variability across time and available Earth observing assets.
- DIAS can integrate across sensors using simple image arithmetic, and our tests in Madagascar indicate that integration of more sensors leads to faster high-quality alerts.

Academic Editor: Nikolay S. Strigul

Received: 20 March 2026
Revised: 24 June 2026
Accepted: 26 June 2026
Published: 6 July 2026

Abstract

Generating satellite-based deforestation alerts with actionable latency requires frequent imaging, creating an imperative to use different sensors together. We introduce a simple and open-source framework called the Disturbance Index Alert System (DIAS), which is based upon transformation of imagery from different sources into an interoperable stream of Disturbance Index (DI) values. Whereas most alert systems target divergence of forested pixels from historical states, DIAS targets movement of a pixel's Z-score position relative to the image-wide population of forest pixels along a forest-sensitive axis. This strategy provides the following practical benefits: (1) it reduces the need to process the historical archive; (2) it reduces dependence upon stable sensor calibration; (3) it allows Z-score-based DI values to be combined across sensors; and (4) it accommodates changes to the group of sensors providing measurements. We demonstrated in Madagascar that sensor integration through DIAS can provide more timely alerts than both conventional individual-sensor systems and additive combination of such systems. Across our study sites, using a commercial source of daily imaging (PlanetScope) in conjunction with imagery from public sources (Landsat, Sentinels-1 and -2) allowed high-confidence detection (false alert rate of approximately 20%) of two-thirds of deforestation occurring at 10 m reference pixels within one month; 40% were detected in that timeframe with public data alone. As commercial options for Earth observation proliferate, flexible and computationally lightweight approaches such as DIAS are needed to accommodate diverse and sometimes only loosely calibrated instruments in support of timely forest monitoring.

Keywords: deforestation alerts; PlanetScope; near real-time; commercial imagery

1. Introduction

Deforestation compromises the planet's capacity for natural climate change mitigation and is an existential threat for many forest-obligate species. Forest protection remains difficult in many regions because of a lack of both monitoring and intervention infrastructure. The potential for satellite-based alerting has long been recognized [1], and satellite-based alert systems have helped reduce deforestation across large areas, especially in the Brazilian Amazon [2]. Recognized mechanisms by which alert systems may support sustainability include: (1) strengthened accountability for global commitments; (2) validation of responsible supply chains; (3) empowered forest defenders; (4) provision of consistent decision support for broad-based restoration; and (5) support of policy decisions [3].

The topographic relief and persistent cloud cover of many primary forests present a challenge for remote sensing, and while existing alert systems may identify deforestation events quickly if those events align fortuitously with scheduled imaging and cloud cover, the average latency across many alert systems can be several months. For instance, the Landsat and Sentinel-2 optical sensors that underpin leading deforestation alert systems each went an average of approximately 80 days in 2022 between cloud-free imaging of any given pixel in Masoala National Park in Madagascar (one of the sites of the current study). The alert latency suggested by this rate of observation may be useful for what Tabor and Holland [4] call "targeted response," providing retrospective information about individual events and allowing assessment of broader trends, but it is not sufficient for "rapid response" applications. The detection timeline needed for dispatch of patrols or for emergency response likely varies internationally, but Tabor and Holland suggested a need for sub-monthly detection.

Many prominent alert systems generate updated forest disturbance maps using repeat measurements from a single satellite system, including multispectral imagery from Landsat [5] and Sentinel-2 [6] as well as C-Band radar imagery from Sentinel-1 [7–9]. Some platforms aggregate alerts generated from individual-sensor algorithms. For example, the union of alerts from single-sensor Landsat, Sentinel-1 and Sentinel-2 systems operating in parallel significantly increases alert frequency [10]. Other systems rely upon pre-process harmonization of data from similar sensors, such as NASA's Harmonized Landsat-Sentinel-2 product (HLS) [11], to create a denser time series of imagery to which a single-sensor change detection process can be applied [12].

The advent of time series-based change detection approaches, wherein date-sensitive functions are fitted to all available acquisitions to highlight any divergence of surface measurements from an expected state, has raised new sensor fusion possibilities for deforestation alerts. New algorithms are combining sensor-agnostic normalized Z-scores, calculated as a pixel-level indication of deviation from historical norms, to reduce deforestation alert latency [13–15]. These methods do require computationally intensive time series fitting, however, and their reliance upon historical imagery limits use of newly launched sensors. All of the above approaches also rely upon stable signals provided by robustly calibrated public space missions.

The question of how best to integrate different sensors has been heightened by the emergence of commercial SmallSats. The PlanetScope constellation of 5 kg satellites is an example of this satellite class. Relatively low sensor cost allows the launch of a large number of instruments providing high-resolution (nominally, 3.7 m), multispectral (visible to near-infrared) imaging at an average frequency of approximately an image per day in most places [16]. However, while PlanetScope image pairs have been used to map forest fires in extensively calibrated deep learning contexts [17,18], there have been no studies, to our knowledge, of how to operationally perform daily change detection using an evolving fleet of instruments that lacks the extensive ground calibration measures associated with missions like Landsat [19].

Here, we propose a multi-sensor extension of a Z-score-based image transformation called the Disturbance Index (DI) [20], and we test DI-based alerts from different combinations of sensors both in terms of accuracy and lag following deforestation. We loosely define deforestation here as the loss of tree cover; while tree loss does not always result in land use change, it does often accompany deforestation in places where near real-time detection systems are needed. The DI represents standard deviations away from the local mean forest condition in terms of a forest-sensitive satellite metric; an abrupt DI change in the direction of non-forest can indicate a disturbance (Figure 1). Unlike the time series-based Z-score algorithms mentioned above, which require historical curve-fitting at the pixel level, DI Z-scores rely only upon the difference between the pixel's value and the global mean of forested pixels in the same image, divided by the global standard deviation. The DI has been used extensively [21,22] for forest disturbance detection with the Landsat platform, and here we tested not only extension of the DI to other public and commercial sensors but also the interoperability of multi-source DI scores to create timely deforestation alerts.

We have developed an open-source platform called DIAS [23] (the Disturbance Index Alert System) to support deforestation monitoring using low-latency satellite data on the Google Earth Engine platform [24]. This platform can produce daily browser-based alerts with the potential to provide consistent information for different parties that may be interested in coordinated deforestation response, including forest patrols; national monitoring authorities; international conservation organizations; and auditors working for forest product trading blocks.

In five sample areas across Madagascar's primary forests, we implemented DIAS to integrate DI values from different sensors (Landsat, Sentinel-2, Sentinel-1, and PlanetScope, each resampled to a ground resolution of 10 m) in the context of deforestation detection. Using a sample of reference points recording the date of deforestation (if any) in 2022, we quantified how quickly and accurately multi-sensor DI time series from different groups of sensors would have allowed deforestation alerting by DIAS.

This application highlights the notion that functional interoperability of diverse satellites can be achieved through derived products instead of more exhaustive sensor-to-sensor calibration. Calculation of the DI is computationally lightweight, and deforestation alerting relies simply upon identifying pixels that cross a DI threshold for a given number of consecutive observations. Both the DI threshold and the number of consecutive observations above that threshold needed to generate an alert are customizable (code available: [23]). Here, we required three consecutive DI values above 3.0 based upon ad hoc examination of the DI distribution in local disturbed and undisturbed forests. Masek et al. [25] described automated methods for threshold selection that could be used across larger, diverse landscapes.

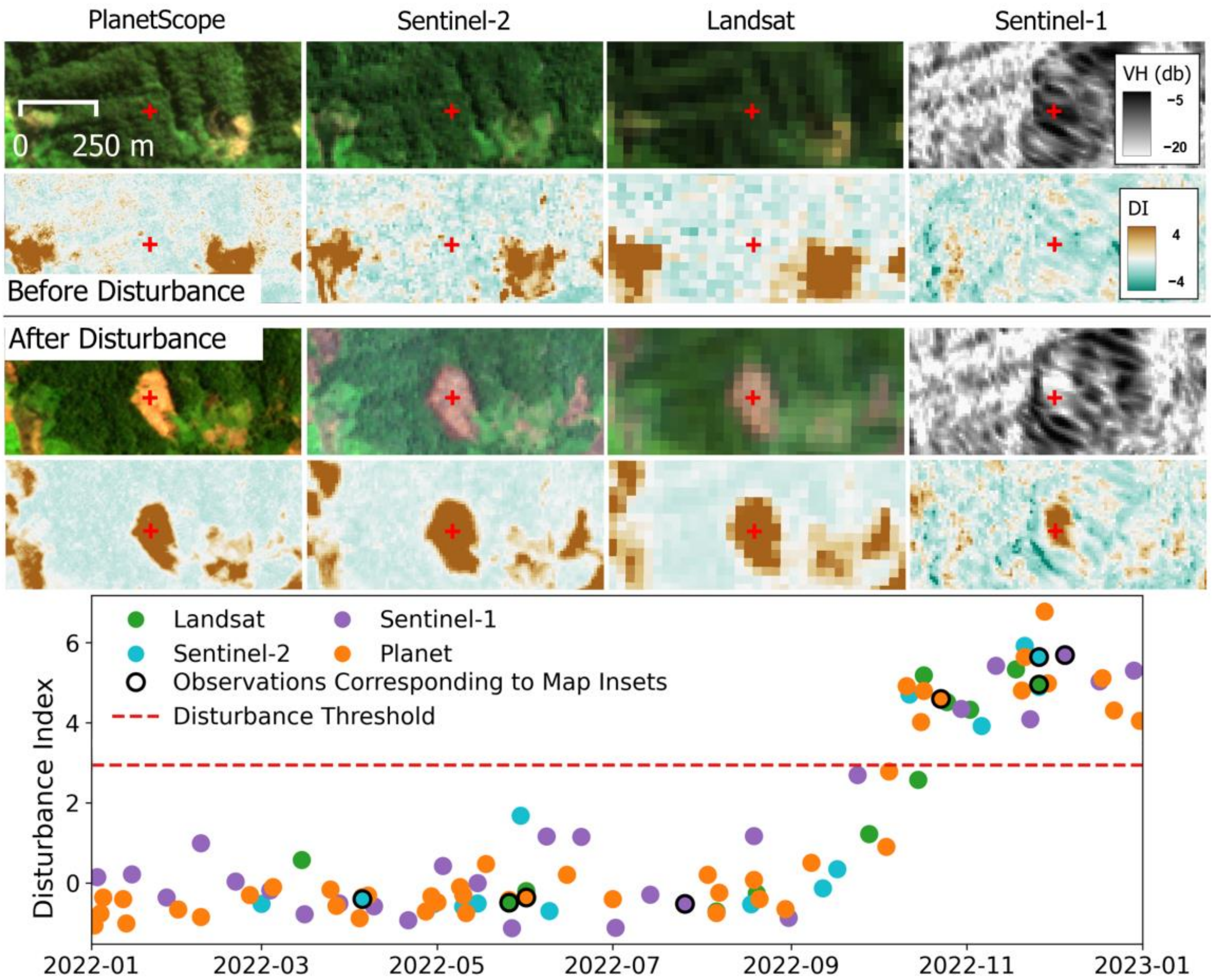

Figure 1. Illustration of multi-sensor deforestation detection based upon sensor-agnostic DI values derived at the location of the red "+". A DI value above 3.0 for three consecutive observations, regardless of originating sensor, triggers an alert. Transformation to DI of imagery from PlanetScope, Sentinel-1, Sentinel-2, and Landsat is described herein.

Transformation to DI does necessarily simplify image data, potentially leading to a loss of signal. This paper tests two hypotheses built into DIAS: (1) that DI values from diverse satellites are sufficiently compatible that accessing more sensors will allow more rapid alerting while committing relatively few false positive errors; and (2) that beyond simply adding more imagery, there is an immediacy benefit to creating a sensor-agnostic stream of images wherein a scene from one satellite can corroborate (or refute) disturbance signal detected in imagery from another.

As Earth-observing sensors proliferate, application-specific interoperability such as we investigate may be a key to both optimizing coverage and maintaining monitoring function across a diverse network of instruments.

2. Materials and Methods

2.1. Sample Data

A total of 1998 sample units were visually interpreted for deforestation date (if any) using all available imagery across 2022 [23]. This stratified random sample was drawn within five 20 × 20 km areas in Eastern Madagascar (Figure 2). These areas each fall within a protected area (Andohahela, Befotaka Midongy, Masoala, and Marojejy National Parks and the Ankeniheny Zahamena Corridor), and they fall along a North–South cloudiness gradient. Strata were designed to maximize sampling of deforestation, appealing to three different change detection methods: RADD [8]; GLAD-L [5]; and Landsat-based disturbance detection with the DI [25]. Allocation of samples was as follows: 12.5% of samples were mapped as deforested in ONLY one of three algorithms (RADD, GLAD-L, DI); 12.5% mapped as deforested by two of three algorithms; 12.5% mapped as deforested by all algorithms; 12.5% no deforestation mapped by any algorithm; 50% no deforestation detected in a 1-pixel buffer around pixels mapped as disturbed by any algorithm. Increasing the number of plots where deforestation was either omitted, erroneously mapped, or detected was designed to support more precise analysis of omission/commission rates as a function of time lag.

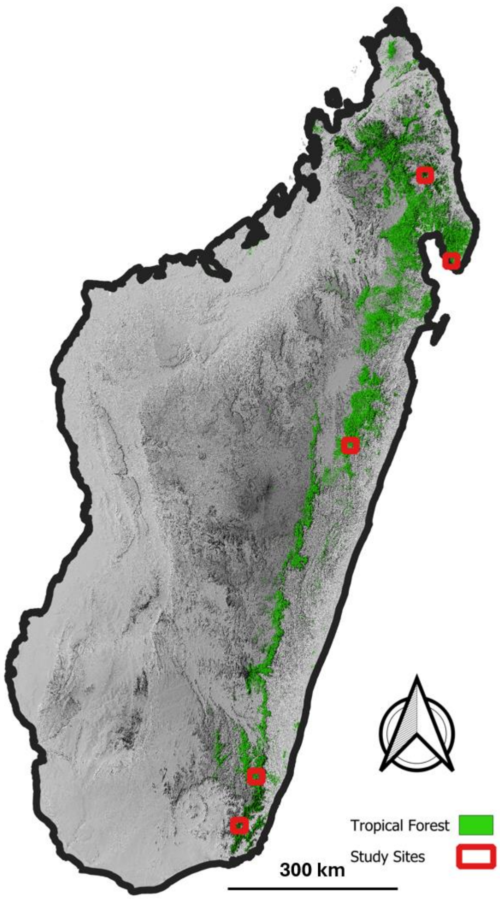

Figure 2. The five study areas in Madagascar where the tests described here were conducted.

At each sample plot, an interpreter visually recorded the date of the first definitive evidence of deforestation throughout calendar year 2022 in a selected 10 m pixel, using the plurality of available imagery from Landsats 7–9, Sentinels 1 and 2, and daily PlanetScope imagery. This deforestation date was the basis of subsequent calculation of alert omission error as a function of lag (time since this recorded disturbance date). Sampling probabilities of each plot, accounting for the above stratification, were used to calculate representative omission and commission errors for each validated map. Sample points falling outside of the forest mask described in the next section (643 plots out of 1998) contributed to calculation of neither omission nor commission error rates because no disturbances could be mapped at those locations, and any observed tree loss in the reference data was assumed to be outside of the domain to which DIAS was being applied. In doing so, we explicitly excluded disturbances in secondary forests, an important system globally that faces its own threats [26]. Results here relate only to moist tropical forests in Madagascar.

2.2. Alert Generation Using the DI

DIAS adapts the DI concept of spatial normalization [20] to interoperably align data from different sensors (Figure 1). Images from different sensors are transformed into comparable units of standard deviations above or below the centroid of the forest population for a given band or index. A Z-score for each forested pixel is determined by dividing the difference between that pixel's value and the mean forest value by the standard deviation for forest pixels within the image. A project-specific 10 m map of Madagascar's primary forests at the beginning of 2022 was used to determine where alerts could be generated. Preliminary analysis showed that accuracy in this mask was paramount because inclusion of previous deforestation sites or agricultural areas led to a high rate of false-positive alerts. The map was created using supervised classification via the Random Forests algorithm [27] applied to a three-month (October–December, 2021) mosaic of Sentinel-2 imagery, using training data acquired visually from PlanetScope and Sentinel-2 sources. This map was also used internally to define the area of forest within each image used to determine the mean and standard deviation of a sensor-specific metric for purposes of the above transformation to DI.

Bands chosen for each sensor as the basis for the above DI calculations were: the Normalized Difference Vegetation Index (contrasting near-infrared and red) for Sentinel-2 and PlanetScope; the Normalized Burn Ratio (contrasting near-infrared and mid-infrared) for Landsat; and the VH (Vertical transmit, Horizontal receive) backscatter band in Ground Range Detected (GRD) scenes from Sentinel-1. There is evidence for VH polarization's superior sensitivity for detecting disturbances in tropical forest canopies compared to VV polarization [28]. Sentinel-1 imagery was pre-processed [29] with a Refined Lee filter (5×5 pixel kernel) and a radiometric slope correction, correcting distortions from varying incidence angles for precise forest structural representation [30]. For PlanetScope, we ingested the orthorectified, 8-band, surface reflectance PlanetScope Scene from Planet's cloud repository into Google Earth Engine [24], where the other datasets were already available.

DIAS treats DI values from different sensors interoperably as a single stream of signals (Figure 1). For this study, DI images were resampled (if necessary) to a standard 10 m resolution using a bilinear method. Native cloud masks were used from each sensor, and the DIAS algorithm created an alert flag for any previously forested pixel that remained at a DI value above 3.0 for at least three consecutive images after being below that value. Multiple independent DI values could be collected and counted on the same day for purposes of consecutive "detections"; this frequently happened across sensors and within the PlanetScope constellation. For purposes of sequence, observations from different sensors on the same day were evaluated in the following order: Sentinel-1, Landsat, Sentinel-2, and Planet.

The exception to strict interoperability was that while a DI value from Sentinel-1 could contribute to the three consecutive values above 3.0 in the generation of an alert, it was not allowed to interrupt a sequence if it was below 3.0. This rule accounted for the fact that the Sentinel-1 DI response to disturbance was generally lower than for the other sensors. Pixels flagged for deforestation were removed on a daily basis from the mask determining where DIAS searched for deforestation. Deforestation flags therefore could occur only once at a given pixel and could not be modified using later imagery. DIAS was applied to every validation pixel using each of the sensor groups identified in Figure 3: (1) Sentinel-1 alone; (2) Landsat alone; (3) Sentinel-2 alone; (4) PlanetScope alone; (5) Landsat and Sentinel-2

https://doi.org/10.3390/rs18132221

together; (6) Landsat, Sentinel-1 and Sentinel-2; (7) PlanetScope, Landsat and Sentinel-2; and (8) all sensors.

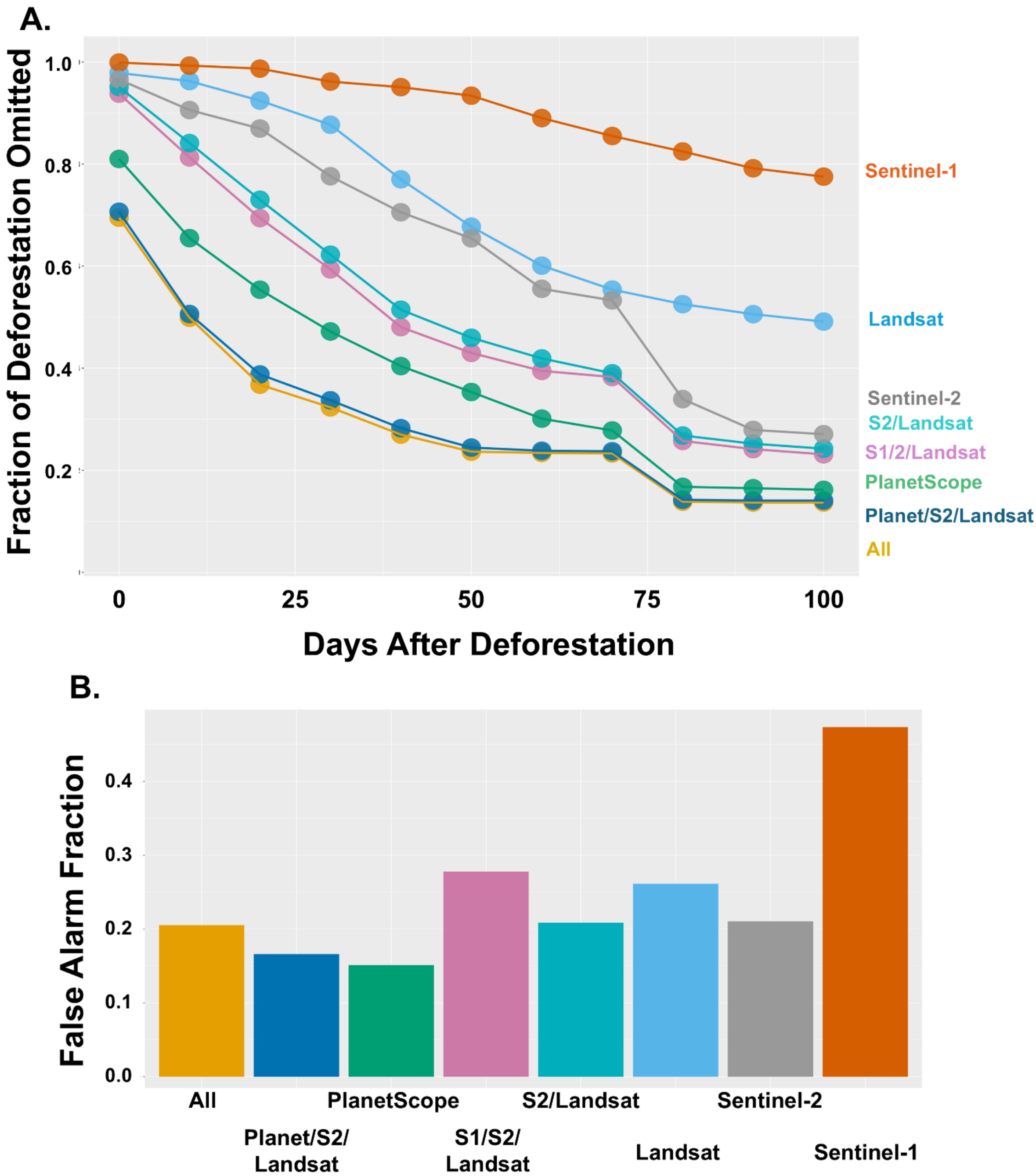

Figure 3. Omission/commission error by sensor. (**A**) Lag is defined in number of days following the first date of clear evidence of deforestation in the reference data. Combinations of sensors in the DIAS framework are indicated with slashes (e.g., Sentinel-2/Landsat). (**B**) Commission error ("false alarm fraction") represents the long-term rate of false-positive alarm pixels as a fraction of all alarm pixels.

2.3. Testing the Effect of Cross-Sensor Corroboration

It is common for change detection algorithms to use multiple post-disturbance images to build alert confidence (e.g., [5,31]). In a multi-sensor context, however, the best way to integrate signal from different sensors remains an open question. A current state-of-the-art alert system operated by Global Forest Watch (GFW) uses the union of alerts created by parallel single-sensor detection systems to accelerate deforestation mapping [10,32]. As we discuss later, the single-sensor systems used by GFW require at least two "detections" prior to generating a high-confidence alert that might then be combined with alerts from other sensors to create a highest-confidence alert [33]. In that system, imagery from different sensors do not corroborate each other directly; multiple sensors are only used together when each has enough "detections" to generate an alert of their own.

By contrast, DIAS allows direct corroboration across sensors because of the interoperability introduced through cross-sensor transformation to DI. We used our reference data to perform a simple test of the impact of this difference. Using the same change detection logic (DI > 3.0 for three images in a row) to declare an alert, we tested two algorithms: (1) generating an alert for all reference data points as soon as either Landsat or Sentinel-2 produced 3 DI values in a row above 3.0; and (2) generating an alert as soon as the integrated stream of DI images from both sensors produced 3 sequential DI values above 3.0. Neither scenario represents a particular operational alert system, but by keeping the detection logic and available imagery constant, we intended to quantify the advantage of allowing corroboration among sensors at the image level instead of at the level of high-confidence alerts.

For each approach, we calculated F_1 scores as a function of post-disturbance lag. An F_1-Score is the harmonic mean of a model's precision and recall, which may also be expressed as

$$F_1 = \frac{2 \times (1 - Omission) \times (1 - Commission)}{(1 - Omission) + (1 - Commission)}$$

Omission and commission error rates were calculated as described in the next section. We performed a bootstrapping-based significance test of the difference in F_1 scores at different levels of time lag (0, 10, . . . 100 days) using the following procedure. In each of 1000 simulations, we resampled with replacement our reference sample and recalculated the weighted omission and commission error rates. These rates were used to calculate F_1, as above, and the simulation-wise F_1 difference was recorded. One of the two integration approaches (integrated stream vs. union of single sensor alerts) was determined to be significantly more accurate ($p < 0.05$) at a given level of lag if its F_1 score was higher in more than 95% of the simulations.

2.4. Testing the Effects of Adding Sensors Through DIAS

For all DI-based sensor combinations within DIAS, listed at the end of Section 2.2, sample points with a deforestation event were considered to be errors of omission from the time of the event until an alert was generated for that specific 10 m pixel. Omission error rates (1 minus the ratio of detected deforestation points/total deforestation points) could thus be evaluated across deforested plots at every level of lag (i.e., number of days since the date of disturbance). Only sample points falling within the project's 2022 primary forest cover mask were used in the calculation of omission and commission rates. In some cases, one or more images with a DI value above the critical threshold of 3.0 were acquired slightly before the deforestation date recorded through image interpretation. This was considered a consequence of DI sometimes being more sensitive to the occurrence of deforestation than a human interpreter. In some cases, the DI value above the threshold prior to the reference date may have been from Sentinel-1, which can be difficult to interpret visually, or from Landsat, the coarser native resolution of which can make it difficult to unambiguously assign a disturbance date to a 10 m reference pixel. For purposes of omission rate calculation, DI values greater than 3.0 from up to 14 days prior to the recorded event were allowed to contribute to the three "detections" needed to generate an alert. This may have artificially reduced omission rates in some cases, but the same rule was applied to all sensor groups being compared. Because the deforestation events recorded in the reference data occurred throughout 2022, each DI-based detection algorithm was operated

100 days into 2023 to ensure that omission rates as a function of lag could be tracked up to 100 days following disturbance.

Rates of commission error (false detections/all detections) were less straightforward to associate with a given level of lag since there was by definition no true event to reference for the timing of false positive errors. Here, we adopted the simplifying assumption that an algorithm's long-term commission rate was an adequate measure of commission at every level of lag. We implemented the design-based weight of every plot (inversely proportional to sampling probability) based on study area and the 5 a priori strata described above under sample design. Specifically, we iteratively (10,000 times) randomly drew with replacement 6000 sample plots, implementing the above-described weights. In each iteration, we calculated the overall commission rate (weighted ratio of false positive alerts/all alerts) for the given algorithm at the end of 2022. The mean weighted commission rate was graphed by algorithm.

3. Results

DIAS alerts created in study areas across Madagascar showed consistent improvements in latency as more sensors were combined, although some sensors contributed more than others (Figure 3). Using PlanetScope imagery alone, more than half of all 10 m deforestation plots were detected within 30 days. At that level of latency, imagery from Sentinel-2 alone supported detection of 21%, Landsat detected 12%, and Sentinel-1 detected 4% (Figure 3; throughout, "detection" is defined as the fraction of 10 m pixel-level deforestation events correctly mapped, while "omission" is 1 minus that fraction). With each of the latter three (public) sensors combined, detection was 41% at 30 days, while inclusion of PlanetScope and the public sensors allowed 30-day detection of 68%.

Omission errors by DIAS across all sensor combinations decreased through the observed 100-day post-disturbance observation period, with omission particularly declining for PlanetScope and Sentinel-2 (and configurations containing those sensors) around the 80-day mark (Figure 3). The period of maximum benefit of PlanetScope in our study area appeared to be between 10 and 30 days following the deforestation event; after that, the difference in omission rate between the "all sensors" and the "all public sensors" DIAS configurations began to decline. By 100 days, the difference in omission rate was only approximately 9% (14% with all sensors and 23% with all sensors except PlanetScope). It was not possible to determine the omission rate of external alert products because historical daily maps for Madagascar in 2022 are not publicly available, but by the end of 2023, the Sentinel 1-based RADD Alert product [8] detected approximately 49% of reference disturbances while the Global Forest Watch Integrated Disturbance Alerts product [33] detected 61%.

Commission error rates, assessed as the fraction of total DIAS alerts that were false after 100 days, were 15% for PlanetScope, 27% for Landsat, 22% for Sentinel-2, and 47% for Sentinel-1. Commission error of DIAS with Sentinel-1/Sentinel-2/Landsat inputs was 7% higher than with just Sentinel-2 plus Landsat; commission was 5% higher when all sensors were used compared to all sensors except Sentinel-1 (Figure 3).

Figure 4 shows that synergy among sensors extended to the local scale. The source of the third sequential DI value above the threshold (the "alert-generating" observation) often varied even within the same patch when all sensors were used together in DIAS. The granularity of sensor integration in this context is partially due to the spatial complexity of available imagery, which was introduced both by the complex orbit patterns of the PlanetScope constellation and by image decimation by clouds. The sensor providing the alert-generating observation may also vary within a patch simply because patches can grow gradually over the course of weeks or months. Figure 4 also shows that while PlanetScope provided a majority of alert-generating observations in all-sensor mode, the other sensors also contributed to the low-latency evident in Figure 3.

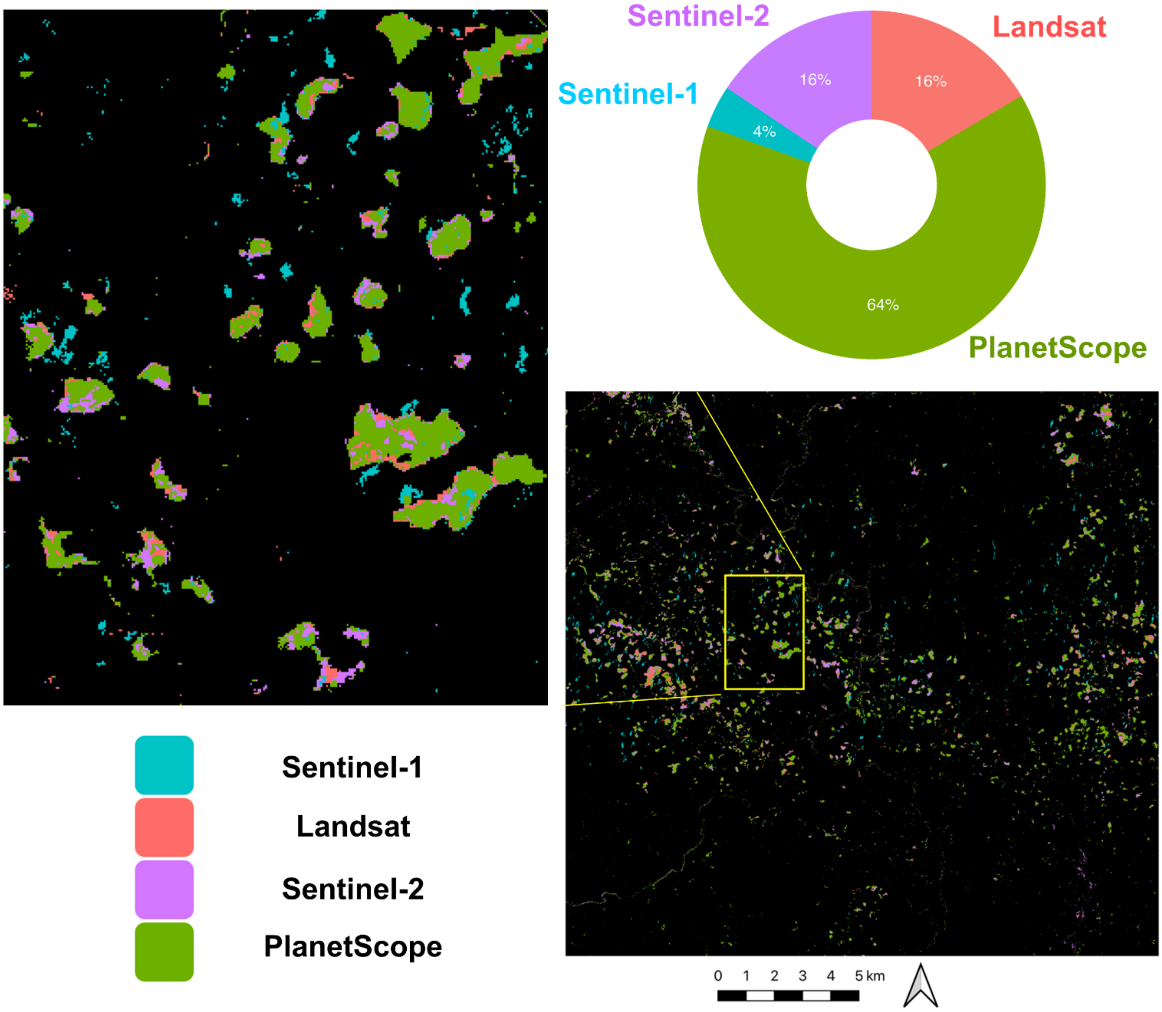

Figure 4. Alerts generated for 2022 by DIAS using all sensors within the central 20 × 20 km study area (see Figure 2). Alerts are indexed in both the overview and inset maps by the sensor that provided the third consecutive "alert-generating" DI value above 3.0; the first two of the three required consecutive values above that threshold may have come from other sensors. Even within the same spatial patch, several different sensors work together to generate alerts. The pie graph represents the fraction of deforestation events in the entire reference dataset for which each sensor provided the critical third detection.

In a direct test of the benefits of using a common stream of DI imagery derived from two sensors vs. adopting the union of parallel single-sensor systems, the common stream option showed important advantages in terms of alert latency. Using identical sets of imagery from the Landsat and Sentinel-2 sensors in our study areas in Madagascar, alert generation with integrated DI values showed latency superior to aggregation of alerts from two single-sensor algorithms. The integrated approach had significantly superior F scores, a measure that combines the effects of both omission and commission errors [34], between 10 and 50 days post-disturbance (Figure 5).

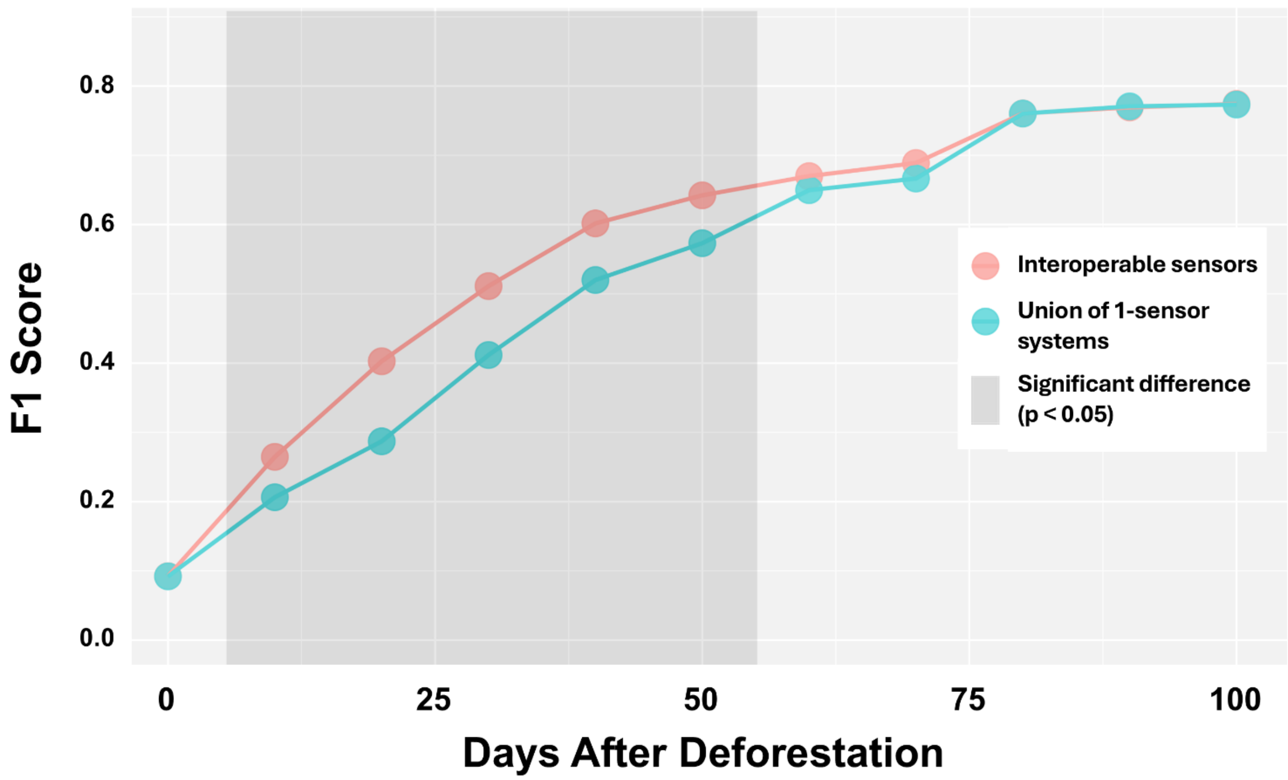

Figure 5. F-scores of alternative sensor fusion methods for Landsat and Sentinel-2. The red series ("Interoperable sensors") represents accuracy of DIAS using Landsat and Sentinel-2 images transformed to a single stream of interoperable DI data to detect deforestation, generating an alert when 3 DI values above 3.0 are acquired consecutively, regardless of sensor. The cyan series ("Union of 1-sensor systems") uses the same imagery and transformation to DI, but an alert is only triggered when the 3 consecutive DI values > 3.0 are acquired by either one sensor or the other. F1 accuracy as a function of post-event lag was calculated using the paper's weighted sample of reference data. The darker gray region indicates the time window since disturbance in which the interoperable approach produced significantly higher accuracy.

4. Discussion

4.1. Alerting Performance by Sensor and Compositing Mechanism

The performance of DIAS reported here should not be taken as globally representative, as several factors affect the latency of alerts in any system. Forest areas in Eastern Madagascar are particularly cloudy, having been classified as "low data availability" (Sentinel-2 and Landsat) by Flores et al. [35] and showing clear imaging at the pixel level by PlanetScope only one day in six (see below). This might indicate that our assessed latency might be conservative in relation to other regions, as might the rapid recovery of local forests [36] because of relatively short windows of unvegetated surface features. On the other hand, separation of forest from non-forest conditions with respect to the Disturbance Index is generally more consistent in systems with dense canopies such as those in Eastern Madagascar; accuracy in more open forests is often lower [20,25]. Differentiation and accuracy may also be compromised if DIAS were to be applied in the detection of more subtle forest cover changes or if used only with coarse-resolution imagery that incompletely resolves canopy removal. Local performance testing would therefore be appropriate whenever DIAS is integrated into a rapid response system.

The many disturbed pixels within a deforestation patch represent multiple opportunities to generate an alert that authorities might use to mobilize a response [37]. Some accuracy assessment approaches have therefore treated an entire patch as "detected" if an alert is generated for any constituent pixel. Our 10 m point-based accuracy assessment likely understated alert accuracy in relation to studies targeting patch-level detection. However, patches may develop over weeks or months, causing ambiguity in the kind of lagging accuracy analysis that interests us here.

Figure 3 clearly shows that adding imagery from more sensors in DIAS generally resulted in gains in alert latency. The speed of detection across sensors was correlated to a degree with imaging frequency. PlanetScope, which by itself supported better detection (with lower commission errors) than the aggregation of the public satellites, provided 62 clear views of the average pixel in our study area in 2022. Landsat (including Landsat missions 7–9) had 15 clear looks, Sentinel-2 had 12, and Sentinel-1 had 28.

Despite regular imaging in the presence of clouds, Sentinel-1 contributed relatively little by way of detection (Figure 4). There is evidence that the sensor's C-band radar is not optimal for immediate detection of tree felling [38], perhaps because of scattering related to logging debris. L-band imagery from the new NISAR platform is likely to be more sensitive to the cutting of trees [15] and represents a potentially important future asset for DIAS. While the additional complexity and processing involved with using Sentinel-1 argue against its inclusion in future iterations of DIAS, it did result in marginal improvements in alert latency when paired with Landsat and Sentinel-2, particularly in the first 70 days following cutting (Figure 3). In light of relatively high rates of commission error (Figure 3), though, use of Sentinel-1 in a DIAS framework may not be merited. Information provided by Sentinel-1, or any of the sensors, may vary across global settings, as may operational sensitivity to marginal improvements in alert timing.

4.2. Application-Specific Sensor Fusion

DIAS likely offers few accuracy-related advantages beyond the near real-time response horizon. Comparison of long-term detection rates (after 100 days with DIAS and after at least a year of monitoring with long-term GFW and RADD products) did not suggest a striking difference between DIAS and other leading algorithms for retrospective purposes. The omission rate of DIAS run with just Sentinel-1 was 78% and dropping steadily at 100 days; it is conceivable that, if allowed to run for a year, omission rates may have approximately matched the omission of the long-term RADD product (51%). The omission error rate of DIAS run with Landsat/Sentinel-1/Sentinel-2 in our study area was 23% after 100 days, which was marginally better than the rate (39%) of the long-term Integrated GFW product that uses the same sensors.

However, in the days and weeks following an event, DIAS has two important advantages: (1) it can be used to pull in additional sensors to accelerate detection, which is evident in Figure 3; and (2) its conversion of imagery from different sources to a single stream of DI values allows different sensors to "corroborate" each other. The logic used by Global Forest Watch's current disturbance alert product [33] illustrates this latter advantage. Four separate algorithms, each operating upon imagery from a single source (Sentinel-1, Landsat, Sentinel-2, and Harmonized Landsat/Sentinel-2), search for disturbance signals in each new image in their respective data streams. "Highest confidence" alerts are issued when more than one system issues a "high confidence" alert. Such an alert depends upon acquisition of at least two corroborative images within a single sensor's data stream. With DIAS, corroborative images (we require three in this paper) may come from any of the input satellites. Figure 5 shows that, with input images and the change detection algorithm held constant, this simple advantage produced significantly better results for our study area in the first 50 days following disturbance.

The DIST-ALERT algorithm [12] likely benefits from the above dynamic, as it uses data from Landsat and Sentinel-2 that have been made interoperable through the Harmonized

Landsat-Sentinel (HLS) process [11]. However, production of HLS requires significantly more computing and storage than the relatively simple distillation of each image to a single-band DI image, and more importantly, it does not offer a route to including other data sources such as PlanetScope. Sensor fusion is a complex topic with many potential practical complications [39], but in the narrow application of issuing deforestation alerts, our experience in Madagascar suggests that simple reduction of multi-sensor imagery to a Z-score conditional on the local forest population is sufficient for effective harmonization.

4.3. Implications for DIAS and Practical Deforestation Alerting

Licensing costs of commercial imagery are a key consideration. In areas where deforestation is unlikely, or where prompt intervention is not a priority, integration of open data sources may be adequate. Image costs should also be considered in the context of broader intervention costs. Surveys emphasize the importance of local staff who are well trained, coordinated, and equipped appropriately for responding to forest threats [40,41]. The cost of providing fresher alerts to local personnel may in some cases be small relative to needed investments in human capital.

Using the Disturbance Index for sensor fusion has several practical advantages. It is based upon simple global mean and standard deviation calculations, limiting computational overhead to the degree that Masek et al. [25] were able to use it to map forest disturbance across North America with 2006 technology. Unlike time series approaches also based upon Z-scores, DIAS requires no historical imagery or intensive time series analysis. Python code (current version: 3.14.6) associated with this paper [23] illustrates the primary functions needed for continuous monitoring, including calculation of DI imagery, tracking of DI scores, and alert generation, on Google Earth Engine (GEE; [24]). These simple functions could be implemented on any platform with access to low-latency imagery, essentially enabling a local instance of DIAS.

Operational tests of the DIAS platform on GEE [23] using Landsat and Sentinel-2 across Madagascar have shown that it can be implemented in real time at scale. We have also verified that the Planet Data API can be used to automatically move daily imagery into a Google Cloud bucket that is accessible by our DI-based change detection algorithm. Similar operations could likewise integrate public datasets not currently on GEE (e.g., [42]). Our test implementation used simple GEE user interface tools, but further front-end development could catalog and distribute alerts to any combination of enforcement staff, regulatory staff, and/or funding agencies.

The choice of ancillary forest maps to be used with DIAS is an impactful decision. In the choice of where DIAS looks for change, our experience indicates that inclusion of non-forest areas (e.g., agricultural zones) quickly generates alerts because such areas undergo rapid changes in vegetation, including transition to states represented by high DI values. Commission error rates are highly sensitive to out-of-date and/or inaccurate land use maps, and use of DIAS for mobilization of interdiction efforts would therefore merit project-specific production of the kind of contemporary, high-quality resource maps we used here.

The other important map-related decision relates to the population used within each acquired image to normalize the population for purposes of calculating DI. Earlier operational uses of the DI with Landsat for forest change detection have defined this normalization population at coarse spatial resolutions and without regard to local-scale variation in forest types [21,25]. However, derivation of population parameters when diverse forest types occur within the same image may result in a loss of sensitivity to change in some places and super-sensitivity in others. Case-specific forest type maps could enable parallel calculation of DI values, but splitting the population within the already-small extent of most high-resolution imagery will sometimes lead to a small number of pixels driving DI normalization. More research is needed related to the sensitivity of DIAS latency and accuracy when this happens.

The self-normalizing property of DI would seem to be relatively robust against inconsistent sensor performance either across time or across different instruments in the same constellation. The aging Landsat 7 satellite provided an informal opportunity to evaluate that idea. Landsat 7 provided 36% of the 2022 Landsat inputs used here despite the fact that the sensor's altitude was lowered by 8 km four months into the study period and a degrading orbit resulted in increasingly early local imaging times [43]. Nevertheless, in the all-sensor implementation of DIAS, Landsat provided the alert-generating observation for the same number of true disturbances as Sentinel-2 (Figure 4), and omission/commission rates were only marginally worse than Sentinel-2 at most levels of lag (Figure 3) despite a ground field of view 9 times coarser. Tracking the departure of a pixel from normal local forest conditions, as DIAS does with every image from every sensor, may reduce dependency upon consistent absolute calibration. In an alerting paradigm where vital frequent imaging is enabled by inexpensive SmallSats of varying ages, this simplicity would represent a tangible operational benefit.

While many current forest protection mechanisms in developing countries do not rely upon, and could not exploit, near real-time deforestation alerting, the emergence of commercial daily imagery and the multi-sensor interoperability we demonstrate signal the feasibility of responding to forest loss in much less time than systems depending upon acquisition of multiple post-event images by a single sensor. The DI-based alerting structure outlined here is: opportunistic with respect to available sensors; computationally lightweight; easily automated; and transparent/replicable for purposes of law enforcement. As options for Earth-observing satellites continue to evolve, this kind of sensor-agnostic alerting may prove optimal for both reducing latency and maintaining stable monitoring systems.

5. Conclusions

DIAS provides a multi-sensor platform for operationally combining imagery from diverse sensors to improve the immediacy of accurate deforestation alerts. As might be expected from daily high-resolution imaging, Planetscope alone provided more immediate alerts in our study area than all of the other sensors used together. However, synergistic combination of public sources through DIAS greatly improved alert latency beyond alerts drawn from any single sensor, and deforestation detection with combined public sensors at approximately 80 days post-event was nearly equivalent to the rate of DIAS driven by those sensors plus PlanetScope. Of particular interest in bandwidth-limited settings, cross-sensor interoperability under DIAS does not depend upon complex time series functions or access to large historical databases. Image inputs need only be "flattened" to a single DI band dependent upon local mean and variance calculations for radiance values, which can often be computed through the programming interfaces used to access low-latency imagery. Change detection under DIAS is a matter of generating an alert when a DI value from any source exceeds a pre-defined threshold for a given number of acquisitions (here, three images in a row). While the costs of integrating commercial data may restrict its use to high-sensitivity settings such as the threatened parks studied here, DIAS' sensor-agnostic change detection logic could provide for seamless alerting across space and variable constellations of available satellites.

https://doi.org/10.3390/rs18132221

Author Contributions: Conceptualization—Z.Y., E.L.B., C.A., and S.P.H. Methodology—Z.Y., E.L.B., E.J.L., and S.P.H. Software—Z.Y., and E.L.B. Validation—E.L.B. Analysis—Z.Y., and E.L.B. Writing/Editing—Z.Y., E.L.B., E.J.L., C.A., and S.P.H. Project Administration—S.P.H. All authors have read and agreed to the published version of the manuscript.

Funding: Support for this research was provided by Grant 80HQTR21T0020 from the NASA Land Cover and Land Use Change Program. The United Nations Food and Agriculture Organization provided licensing for the PlanetScope archive.

Data Availability Statement: Disturbance reference data and Python code representing basic I/O and alert-generating logic for DIAS: https://zenodo.org/records/17792386 (accessed on 1 June 2026) [23].

Acknowledgments: The authors appreciate guidance from Andreas Vollrath, Andriambolantsoa Rasolohery, and Syliva Wilson. The findings and conclusions in this publication are those of the authors and should not be construed to represent any official USDA or U.S. Government determination or policy.

Conflicts of Interest: The authors declare no conflicts of interest.

References

1. Williams, D.L.; Miller, L.D. Monitoring Forest Canopy Alteration Around the World with Digital Analysis of Landsat Data. In *Monitoring Forest Canopy Alteration Around the World with Digital Analysis of Landsat Imagery*; Williams, D.L., Miller, L.D., Eds.; Goddard Space Flight Center: Greenbelt, MD, USA, 1979; pp. 1–3.
2. Assunção, J.; Gandour, C.; Rocha, R. DETER-ing Deforestation in the Amazon: Environmental Monitoring and Law Enforcement. *Am. Econ. J. Appl. Econ.* **2023**, *15*, 125–156. [CrossRef]
3. Shae, K. Measuring the impact of monitoring: How we know transparent near-real time data can help save the forests. In *Transformational Change for People and the Planet*; Uitto, J.I., Batra, G., Eds.; Springer: Berlin/Heidelberg, Germany, 2022; pp. 263–273.
4. Tabor, K.M.; Holland, M.B. Opportunities for improving conservation early warning and alert systems. *Remote Sens. Ecol. Conserv.* **2021**, *7*, 7–17. [CrossRef]
5. Hansen, M.C.; Krylov, A.; Tyukavina, A.; Potapov, P.V.; Turubanova, S.; Zutta, B.; Ifo, S.; Margono, B.; Stolle, F.; Moore, R. Humid tropical forest disturbance alerts using Landsat data. *Environ. Res. Lett.* **2016**, *11*, 034008. [CrossRef]
6. Pacheco-Pascagaza, A.M.; Gou, Y.; Louis, V.; Roberts, J.F.; Rodríguez-Veiga, P.; da Conceição Bispo, P.; Espírito-Santo, F.D.B.; Robb, C.; Upton, C.; Galindo, G.; et al. Near Real-Time Change Detection System Using Sentinel-2 and Machine Learning: A Test for Mexican and Colombian Forests. *Remote Sens.* **2022**, *14*, 707. [CrossRef]
7. Kilbride, J.B.; Poortinga, A.; Bhandari, B.; Thwal, N.S.; Quyen, N.H.; Silverman, J.; Tenneson, K.; Bell, D.; Gregory, M.; Kennedy, R.; et al. A Near Real-Time Mapping of Tropical Forest Disturbance Using SAR and Semantic Segmentation in Google Earth Engine. *Remote Sens.* **2023**, *15*, 5223. [CrossRef]
8. Reiche, J.; Mullissa, A.; Slagter, B.; Gou, Y.; Tsendbazar, N.-E.; Odongo-Braun, C.; Vollrath, A.; Weisse, M.J.; Stolle, F.; Pickens, A.; et al. Forest disturbance alerts for the Congo Basin using Sentinel-1. *Environ. Res. Lett.* **2021**, *16*, 024005. [CrossRef]
9. Silva, C.A.; Guerrisi, G.; Del Frate, F.; Sano, E.E. Near-real time deforestation detection in the Brazilian Amazon with Sentinel-1 and neural networks. *Eur. J. Remote Sens.* **2022**, *55*, 129–149. [CrossRef]
10. Reiche, J.; Balling, J.; Pickens, A.H.; Masolele, R.N.; Berger, A.; Weisse, M.J.; Mannarino, D.; Gou, Y.; Slagter, B.; Donchyts, G.; et al. Integrating satellite-based forest disturbance alerts improves detection timeliness and confidence. *Environ. Res. Lett.* **2024**, *19*, 054011. [CrossRef]
11. Claverie, M.; Ju, J.; Masek, J.G.; Dungan, J.L.; Vermote, E.F.; Roger, J.C.; Skakun, S.V.; Justice, C. The Harmonized Landsat and Sentinel-2 surface reflectance data set. *Remote Sens. Environ.* **2018**, *219*, 145–161. [CrossRef]
12. Pickens, A.H.; Hansen, M.C.; Song, Z.; Poulson, A.; Komarova, A.; Baggett, A.; Kerr, T.; Mikus, A.; Ortiz Dominguez, C.; Tyukavina, A.; et al. Rapid monitoring of global land change. *Nat. Commun.* **2025**, *16*, 8948. [CrossRef] [PubMed]
13. Tang, X.; Bratley, K.H.; Cho, K.; Bullock, E.L.; Olofsson, P.; Woodcock, C.E. Near real-time monitoring of tropical forest disturbance by fusion of Landsat, Sentinel-2, and Sentinel-1 data. *Remote Sens. Environ.* **2023**, *294*, 113626. [CrossRef]
14. McGregor, I.R.; Connette, G.; Gray, J.M. A multi-source change detection algorithm supporting user customization and near real-time deforestation detections. *Remote Sens. Environ.* **2024**, *308*, 114195. [CrossRef]
15. Flores-Anderson, A.I.; Cardille, J.A.; Kellndorfer, J.; Meyer, F.J.; Olofsson, P. Early Deforestation Detection in the Tropics using L-band SAR and Optical multi-sensor data and Bayesian Statistics. *Int. J. Appl. Earth Obs. Geoinf.* **2025**, *143*, 104831. [CrossRef]
16. Roy, D.P.; Huang, H.; Houborg, R.; Martins, V.S. A global analysis of the temporal availability of PlanetScope high spatial resolution multi-spectral imagery. *Remote Sens. Environ.* **2021**, *264*, 112586. [CrossRef]

17. Martins, V.S.; Roy, D.P.; Huang, H.; Boschetti, L.; Zhang, H.K.; Yan, L. Deep learning high resolution burned area mapping by transfer learning from Landsat-8 to PlanetScope. *Remote Sens. Environ.* **2022**, *280*, 113203. [CrossRef]
18. Kim, B.; Lee, K.; Park, S. Burned-Area Mapping Using Post-Fire PlanetScope Images and a Convolutional Neural Network. *Remote Sens.* **2024**, *16*, 2629. [CrossRef]
19. Czapla-Myers, J.; McCorkel, J.; Anderson, N.; Thome, K.; Biggar, S.; Helder, D.; Aaron, D.; Leigh, L.; Mishra, N. The Ground-Based Absolute Radiometric Calibration of Landsat 8 OLI. *Remote Sens.* **2015**, *7*, 600–626. [CrossRef]
20. Healey, S.P.; Cohen, W.B.; Zhiqiang, Y.; Krankina, O.N. Comparison of Tasseled Cap-based Landsat data structures for use in forest disturbance detection. *Remote Sens. Environ.* **2005**, *97*, 301–310. [CrossRef]
21. Healey, S.P.; Cohen, W.B.; Spies, T.A.; Moeur, M.; Pflugmacher, D.; Whitley, M.G.; Lefsky, M. The relative impact of harvest and fire upon landscape-level dynamics of older forests: Lessons from the Northwest Forest Plan. *Ecosystems* **2008**, *11*, 1106–1119. [CrossRef]
22. Wegler, M.; Thonfeld, F.; Asam, S.; Kacic, P.; Kuenzer, C. Tree species–specific forest canopy cover loss in Germany (2018–2024): A national-scale remote sensing assessment. *For. Ecol. Manag.* **2026**, *609*, 123630. [CrossRef]
23. Healey, S.P.; Yang, Z.; Bullock, E. Code and Reference Data for DIAS (Disturbance Index Alert System) in Madagascar. 2025. Available online: https://zenodo.org/records/17792386 (accessed on 1 June 2026).
24. Gorelick, N.; Hancher, M.; Dixon, M.; Ilyushchenko, S.; Thau, D.; Moore, R. Google Earth Engine: Planetary-scale geospatial analysis for everyone. *Remote Sens. Environ.* **2017**, *202*, 18–27. [CrossRef]
25. Masek, J.G.; Huang, C.; Wolfe, R.; Cohen, W.; Hall, F.; Kutler, J.; Nelson, P. North American forest disturbance mapped from a decadal Landsat record. *Remote Sens. Environ.* **2008**, *112*, 2914–2926. [CrossRef]
26. Ngo Bieng, M.A.; Souza Oliveira, M.; Roda, J.-M.; Boissière, M.; Hérault, B.; Guizol, P.; Villalobos, R.; Sist, P. Relevance of secondary tropical forest for landscape restoration. *For. Ecol. Manag.* **2021**, *493*, 119265. [CrossRef]
27. Breiman, L. Random Forests. *Mach. Learn.* **2001**, *45*, 5–32. [CrossRef]
28. Reiche, J.; Verhoeven, R.; Verbesselt, J.; Hamunyela, E.; Wielaard, N.; Herold, M. Characterizing Tropical Forest Cover Loss Using Dense Sentinel-1 Data and Active Fire Alerts. *Remote Sens.* **2018**, *10*, 777. [CrossRef]
29. Mullissa, A.; Vollrath, A.; Odongo-Braun, C.; Slagter, B.; Balling, J.; Gou, Y.; Gorelick, N.; Reiche, J. Sentinel-1 SAR Backscatter Analysis Ready Data Preparation in Google Earth Engine. *Remote Sens.* **2021**, *13*, 1954. [CrossRef]
30. Vollrath, A.; Mullissa, A.; Reiche, J. Angular-Based Radiometric Slope Correction for Sentinel-1 on Google Earth Engine. *Remote Sens.* **2020**, *12*, 1867. [CrossRef]
31. Hoekman, D.; Kooij, B.; Quiñones, M.; Vellekoop, S.; Carolita, I.; Budhiman, S.; Arief, R.; Roswintiarti, O. Wide-Area Near-Real-Time Monitoring of Tropical Forest Degradation and Deforestation Using Sentinel-1. *Remote Sens.* **2020**, *12*, 3263. [CrossRef]
32. Doblas Prieto, J.; Lima, L.; Mermoz, S.; Bouvet, A.; Reiche, J.; Watanabe, M.; Sant Anna, S.; Shimabukuro, Y. Inter-comparison of optical and SAR-based forest disturbance warning systems in the Amazon shows the potential of combined SAR-optical monitoring. *Int. J. Remote Sens.* **2023**, *44*, 59–77. [CrossRef]
33. Berger, A.; Carter, S.; Schofield, T.; Pickens, A.; Reiche, J. Looking for the Quickest Signal of Deforestation or Vegetation Disturbance Globally? Turn to GFW's Integrated Disturbance Alerts. Available online: https://www.globalforestwatch.org/blog/data-and-tools/integrated-deforestation-alerts/ (accessed on 17 June 2026).
34. Bullock, E.L.; Healey, S.P.; Yang, Z.; Houborg, R.; Gorelick, N.; Tang, X.; Andrianirina, C. Timeliness in Forest Change Monitoring: A New Assessment Framework Demonstrated using Sentinel-1 and a Continuous Change Detection Algorithm. *Remote Sens. Environ.* **2022**, *276*, 113043. [CrossRef]
35. Flores-Anderson, A.I.; Cardille, J.; Azad, K.; Cherrington, E.; Zhang, Y.; Wilson, S. Spatial and Temporal Availability of Cloud-free Optical Observations in the Tropics to Monitor Deforestation. *Sci. Data* **2023**, *10*, 550. [CrossRef] [PubMed]
36. Armstrong, A.; Fischer, R.; Huth, A.; Shugart, H.; Fatoyinbo, T. Simulating Forest Dynamics of Lowland Rainforests in Eastern Madagascar. *Forests* **2018**, *9*, 214. [CrossRef]
37. Tang, X.; Bullock, E.L.; Olofsson, P.; Estel, S.; Woodcock, C.E. Near real-time monitoring of tropical forest disturbance: New algorithms and assessment framework. *Remote Sens. Environ.* **2019**, *224*, 202–218. [CrossRef]
38. Hethcoat, M.G.; Carreiras, J.M.B.; Bryant, R.G.; Quegan, S.; Edwards, D.P. Combining Sentinel-1 and Landsat 8 Does Not Improve Classification Accuracy of Tropical Selective Logging. *Remote Sens.* **2022**, *14*, 179. [CrossRef]
39. Samadzadegan, F.; Toosi, A.; Dadrass Javan, F. A critical review on multi-sensor and multi-platform remote sensing data fusion approaches: Current status and prospects. *Int. J. Remote Sens.* **2025**, *46*, 1327–1402. [CrossRef]
40. Musinsky, J.; Tabor, K.; Cano, C.A.; Ledezma, J.C.; Mendoza, E.; Rasolohery, A.; Sajudin, E.R. Conservation impacts of a near real-time forest monitoring and alert system for the tropics. *Remote Sens. Ecol. Conserv.* **2018**, *4*, 189–196. [CrossRef]
41. Slough, T.; Kopas, J.; Urpelainen, J. Satellite-based deforestation alerts with training and incentives for patrolling facilitate community monitoring in the Peruvian Amazon. *PNAS* **2021**, *118*, e2015171118. [CrossRef] [PubMed]

42. Picoli, M.C.A.; Simoes, R.; Chaves, M.; Santos, L.A.; Sanchez, A.; Soares, A.; Sanches, I.D.; Ferreira, K.R.; Queiroz, G.R. Cbers Data Cube: A Powerful Technology for Mapping and Monitoring Brazilian Biomes. *ISPRS Ann. Photogramm. Remote Sens. Spat. Inf. Sci.* **2020**, *V-3-2020*, 533–539. [CrossRef]
43. USGS. *Landsat 7 (L7) Data Users Handbook, v3*; USGS: Sioux Falls, SD, USA, 2024; Volume LSDS-1927.